

C. M. Arndt, C. Dem, W. Meier

Influence of Fuel Staging on Thermo-Acoustic Oscillations in a Premixed Stratified Dual-Swirl Gas Turbine Model Combustor

Flow, Turbulence and Combustion 106 (2021), 613-629.

The original publication is available at [www.springerlink.com](http://www.springerlink.com)

<http://dx.doi.org/10.1007/s10494-020-00158-6>

# **Influence of Fuel Staging on Thermo-Acoustic Oscillations in a Premixed Stratified Dual-Swirl Gas Turbine Model Combustor**

C. M. Arndt\*, C. Dem, W. Meier

German Aerospace Center (DLR), Institute of Combustion Technology  
Pfaffenwaldring 38-40, 70569 Stuttgart, Germany

\* corresponding author: christoph.arndt@dlr.de

ORCID

Christoph Arndt: 0000-0003-0871-6620

Wolfgang Meier: 0000-0002-1752-1246

## **Abstract**

In several technical combustion systems for lean, premixed combustion, mixture stratification plays an important role, such as in stationary and aero gas turbines. The current paper focuses on a detailed characterization of a dual-swirl gas turbine model combustor operated in a stratified regime. The influence of mixture stratification on flame stabilization and self-induced thermo-acoustic oscillations was studied using laser and optical diagnostics in combination with microphone probes to measure pressure oscillations in the plenums and combustion chamber. The overall flame-shape was imaged using OH\* chemiluminescence. Laser Raman scattering was applied to study the thermo-chemical state of the flame, the flow-field was measured using Particle Image Velocimetry and pressure oscillations in the combustion chamber and in the air plenums were determined by using calibrated microphone probes. OH planar laser-induced fluorescence was used to determine fluctuations of the hot gas with high spatial resolution. Significant mixture stratification within the combustion chamber was found to only occur at or upstream of the flame root. Varying the stratification level did not significantly influence the mean flame shape and flow field, however, a clear influence on thermo-acoustic oscillations was observed.

## **Keywords**

Laser Diagnostics, Stratified Combustion, Gas Turbine Model Combustor, Thermo-Acoustics

## Introduction

In gas turbines for land based [1] and aeronautical [2] applications, lean premixed combustion is becoming of increased importance due to the potential for the reduction of pollutants. However, in practical applications, mixture stratification (i.e. non-uniform mixture fraction distributions) can occur, e.g. due to using a pilot stage or due to imperfect mixing, thus influencing the flame stabilization and flame dynamics.

Stratified flames in generic configurations have gained significant research interest in recent years, both experimentally and numerically. For example Sweeney et al. applied laser-based measurements of flow field and species concentration in stratified low turbulence flames in a slot burner [3] and in non-swirling and swirling stratified flames in a double-annular bluff body burner [4,5]. They found significant levels of stratification within the flame front. Seffrin et al. and Kuenne et al. studied a series of flames in a co-annular burner with a flame holder and well-defined boundary conditions, the so-called Darmstadt stratified flame [6,7]. They discovered considerable influence of the operating conditions on the flame topology. Meares et al. [8,9] studied the effect of different levels of mixture fraction inhomogeneities in a co-annular tube burner. Here, mixture inhomogeneities significantly influenced the stabilization limit of the burner.

Several of these configurations have also been studied numerically, and are target flames of the International Workshop on Turbulent Flames (TNF) [10]. A recent overview of experiments and simulations of stratified flames is given in the review paper by Masri [11]. Besides the above mentioned simple stratified flame configurations, several other model combustors with technically premixed flames, resulting in flames with mixture stratification, are described in the literature (e.g. [12-14]).

In the current study, stratified flames are investigated in the SFB 606 dual-swirl gas turbine model combustor (GTMC), which provides a technically relevant geometry (i.e. swirl, high turbulence levels and thermal powers, enclosed flame). The burner features two concentric co-rotating swirlers, each supplied by a separate plenum, allowing to feed each of the two concentric flows with premixed mixtures of different equivalence ratios. This GTMC has been studied previously with focus on technically premixed methane flames [15-17] and prevaporized liquid fuel flames [18,19]. A nearly identical setup

is available for liquid fuels [20]. Further, the design allows for several identical burners to be combined into a combustor array, in order to investigate cross-flame interactions [21].

In the current paper, the focus is on a detailed characterization of the influence of stratification on self-excited thermo-acoustic oscillations. Three flames, one perfectly premixed flame and two flames with different stratification levels, were studied using laser-based and optical measurement techniques. The flow-fields were characterized by stereoscopic particle image velocimetry (PIV), the flame shapes were visualized by planar laser-induced fluorescence (PLIF) of OH and OH<sup>\*</sup> chemiluminescence imaging, and laser Raman scattering was used to determine the thermo-chemical state of the flames. In addition, microphone probes in the two plenum chambers and in the combustion chamber allowed the assessment of the acoustic boundary conditions. Different acoustic modes of the combustor were excited by the flames and the level of excitation changed with the mixture stratification. The results demonstrate how thermo-acoustic instabilities in gas turbine flames can be influenced by modifying and controlling the mixture stratification.

## Experiment

### *SFB 606 Gas Turbine Model Combustor*

A schematic of the combustor is shown in Figure 1. Details on the geometry can be found in the literature [15], and only a brief overview is provided here. The combustor has two concentric, co-rotating swirlers, each being supplied through a separate plenum chamber. Thus, the gas supply to each plenum (and swirler) can be set independently, allowing control of the air split ratio  $L$  (defined as the ratio of the mass flows of the outer and inner plenum). For the current study, all flames were operated at an air split ratio  $L = 1.6$ , corresponding to equal pressure loss across both swirlers. Different fuel/air mixtures were supplied to each swirler by premixing fuel and air far upstream of the plenum inlets using static mixers (Sulzer).

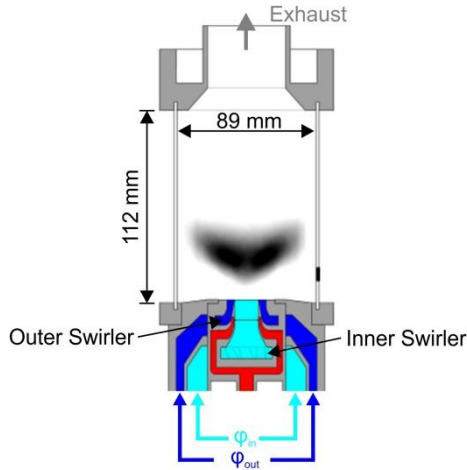


*Figure 1. Schematic of the SFB 606 dual swirl gas turbine model combustor.*

The vertically arranged combustion chamber offers very good optical access from all four sides and is equipped with several ports for dynamic pressure probes.

Table 1 shows the operating conditions. All studied flames had a global equivalence ratio of  $\phi_{global} = 0.75$  and a thermal power of  $P_{th} = 25$  kW. The mixture fraction in the inner and outer plenum was varied, resulting in different stratification ratios  $S$  between 1 (corresponding to a perfectly premixed flame) and 1.67. Here,  $S$  is defined as the ratio of the equivalence ratio in the inner ( $\phi_{in}$ ) and outer ( $\phi_{out}$ ) stream.

Table 1. Operating conditions. All flames are operated at a global equivalence ratio of  $\phi_{\text{global}} = 0.75$  and a thermal power of  $P_{\text{th}} = 25$  kW.  $S$  is the stratification ratio ( $S = \phi_{\text{in}} / \phi_{\text{out}}$ ), the subscripts denote the inner (in) and outer (out) streams.  $\dot{m}$  are the mass flows.

$S$	$\phi_{\text{in}}$	$\phi_{\text{out}}$	Mass Flows / g/min			
			$\dot{m}_{\text{air},\text{in}}$	$\dot{m}_{\text{air},\text{out}}$	$\dot{m}_{\text{CH}_4,\text{in}}$	$\dot{m}_{\text{CH}_4,\text{out}}$
1	0.75	0.75	265	424	11.5	18.4
1.38	0.9	0.65	261	427	13.6	16.3
1.67	1	0.6	258	430	15.0	15.0

Although the stability envelope of the combustor is larger than the operating conditions studied here, the operating conditions were selected to avoid rich mixtures in the inner stream. This would have resulted in unburnt gas ( $\text{H}_2$  and  $\text{CO}$ ) being transported downstream and reacting there with excess  $\text{O}_2$  from the outer stream. Similarly, with the restriction of  $\phi_{\text{in}} \leq 1$ , very lean mixtures in the outer stream ( $\phi_{\text{out}} < 0.6$ ) would have led to a change of the global equivalence ratio.

#### *OH Planar Laser-Induced Fluorescence (PLIF) and $\text{OH}^*$ Chemiluminescence (CL) Imaging*

OH planar laser-induced fluorescence was measured at a frame rate of 10 kHz using a Sirah Credo dye laser pumped by a diode-pumped solid state (DPSS) laser (Edgewave Innoslab IS400-2-L). The frequency doubled output of the dye laser was tuned to 283.2 nm to match the  $\text{Q}_1(7)$  transition of OH in the A-X ( $v'' = 1, v' = 0$ ) band. The laser beam was expanded into a light sheet using a two-stage cylindrical telescope and focused into the test section using a third cylindrical lens, resulting in a laser sheet of approximately 100 mm height with a beam waist in the test section of approximately 0.5 mm. The fluorescence signal in the (1,1) and (0,0) band around 308 nm was collected using a high speed CMOS camera (Phantom V1212) equipped with a two-stage high speed image intensifier (LaVision HS IRO), a Halle  $f = 64$  mm  $f/2$  UV lens and a high transmission ( $T > 80\%$  at 310 nm) band pass filter. A part of the light sheet was directed into a dye cell containing Rhodamine 6G solved in ethanol to correct for shot-to-shot sheet profile and laser energy fluctuations. Fluorescence from the dye cell was imaged using a Photron SA1.1 high-speed CMOS camera equipped with a Nikon Nikkor  $f = 50$  mm  $f/1.4$  lens.

$\text{OH}^*$  chemiluminescence was simultaneously imaged using the same camera / image intensifier combination used for OH PLIF. Here, the camera was operated at a frame rate of 20 kHz with alternating short (300 ns for OH PLIF) and long (15  $\mu\text{s}$  for  $\text{OH}^*$  CL) image intensifier gates, resulting in OH PLIF images for the even camera frames and  $\text{OH}^*$  CL images for the odd camera frames. 30,000 single shot image pairs were recorded for each operating condition. The corresponding trigger scheme for the camera, image intensifier (I/I) and laser is shown in Figure 2.

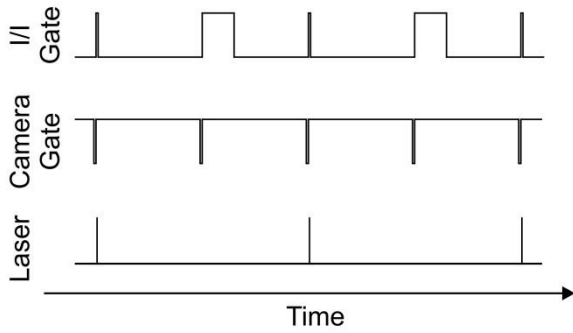


Figure 2. Trigger scheme for the OH PLIF /  $\text{OH}^*$  CL camera and the OH PLIF laser.

The benefit of this setup lies in the reduced optical access necessary for the two measurement quantities and a decreased experimental complexity and cost as well as a perfect, calibration-free, spatial overlap between OH PLIF and  $\text{OH}^*$  CL.

#### *Stereoscopic Particle Image Velocimetry (S-PIV)*

The three-component velocity field in the measurement plane was acquired with Stereoscopic Particle Image Velocimetry (S-PIV) at a repetition rate of 10 kHz. Titanium dioxide particles were added to the flow and illuminated with a frequency doubled dual-head DPSS Nd:YAG laser (Edgewave Innoslab IS200-2-LD, pulse energy 5 mJ at 532 nm, pulse separation time 15  $\mu\text{s}$  - 20  $\mu\text{s}$ , depending on the operating condition). Mie scattering from the particles was recorded with a pair of high speed CMOS cameras (Photron SA5). The cameras were mounted at an angle of 30° relative to the normal of the laser light sheet and were equipped with Tokina  $f = 100$  mm macro lenses (set to  $f/5.6$ ) and band-pass filters (532 $\pm$ 5 nm) to suppress background luminosity of the flame. 30,000 single shot image pairs were recorded for each operating condition and the velocity fields were calculated from the particle images



using a multi-scale cross-correlation PIV algorithm (LaVision DaVis 8.4) with a final interrogation window size of 16 x 16 pixel with 50% overlap. The resulting spatial resolution and vector spacing were 1.3 mm and 0.65 mm, respectively.

Single-shot laser Raman scattering was applied for the pointwise quantitative measurement of the major species concentrations ( $\text{O}_2$ ,  $\text{N}_2$ ,  $\text{CH}_4$ ,  $\text{H}_2$ ,  $\text{CO}$ ,  $\text{CO}_2$ ,  $\text{H}_2\text{O}$ ) and the temperature. Raman measurements were only performed for the operating condition with the highest stratification ratio ( $S = 1.67$ ), as the highest mixture fraction variations are expected here. Details of the measurement system can be found in [14,22] and only a short summary is given here. The radiation of a flashlamp-pumped dye laser (Candela LFDL 20, 1.8 J/pulse at 489 nm, pulse duration 3  $\mu\text{s}$ , pulse repetition rate 5 Hz) was focused into the combustion chamber and the Raman scattering emitted from the measurement volume (length  $\approx 0.6$  mm, diameter  $\approx 0.6$  mm) was collected by an achromatic lens ( $D = 80$  mm,  $f = 160$  mm) and relayed to the entrance slit of a spectrograph (SPEX 1802,  $f = 1$  m, slit width 2 mm, dispersion  $\approx 0.5$  nm/mm). The dispersed and spatially separated signals from the different species were detected by individual photomultiplier tubes (PMTs) in the focal plane of the spectrograph and sampled using boxcar integrators. The species number densities were calculated from these signals using calibration measurements and the temperature was deduced from the total number density via the ideal gas law. The simultaneous detection of all major species with each laser pulse also enabled the determination of the instantaneous mixture fraction [23] following the method by Bilger et al. [24].

400 single-shot Raman measurements per measurement location were performed at a total of 70 measurement locations at axial ( $8 \text{ mm} < z < 80 \text{ mm}$ ) and radial ( $-3 \text{ mm} < x < 27 \text{ mm}$ ) locations. Measurement locations with  $x < 8 \text{ mm}$  and  $z > 27 \text{ mm}$  were not accessible due to clipping of the solid angle of the detection optics.

Systematic uncertainties were typically  $\pm 3 - 4\%$  for the temperature and mixture fraction,  $\pm 3 - 5\%$  for the mole fractions of  $\text{O}_2$ ,  $\text{H}_2\text{O}$ ,  $\text{CO}_2$  and  $\text{CH}_4$ . Because of the low concentrations of  $\text{H}_2$  and  $\text{CO}$  in the flames investigated, the uncertainty is relatively large for these species. These are estimated to be around  $\pm 20\%$  at a mole fraction of 0.01. The statistical uncertainties were approximately 30% larger than stated in a previous study [14] due to a lower pulse energy applied in the current measurements. Typical statistical uncertainties (for a single shot measurement) were 3% for the temperature and mixture fraction, 4% for  $\text{H}_2\text{O}$  and 9% for  $\text{O}_2$  and  $\text{CO}_2$  in the exhaust gas [25,14].

### *Acoustic Measurements*

Pressure oscillations in the combustion chamber and in the two air plenums were measured using calibrated microphone probes (Brüel & Kjær, type 4939), with a sampling rate of 100 kHz. The microphone probes were calibrated for frequencies up to 10 kHz. The pressure power spectrum at each location was computed by slicing the long-duration pressure signal into one-second segments, and calculating the power spectrum for each segment. Afterwards, the spectra of the segments were averaged, resulting in a frequency resolution of 1 Hz. Acoustic modes leading to an asymmetric pressure distribution in the combustion chamber, such as transversal modes or asymmetric flow features like precessing vortex cores (PVCs), can be detected by using the difference signal of two microphone probes mounted on opposite sides of the combustion chamber, but at the same axial position.

## Results and Discussion

### Characterization of the Flames

An overview of the heat release zone for the different studied stratification ratios is given in Figure 3.

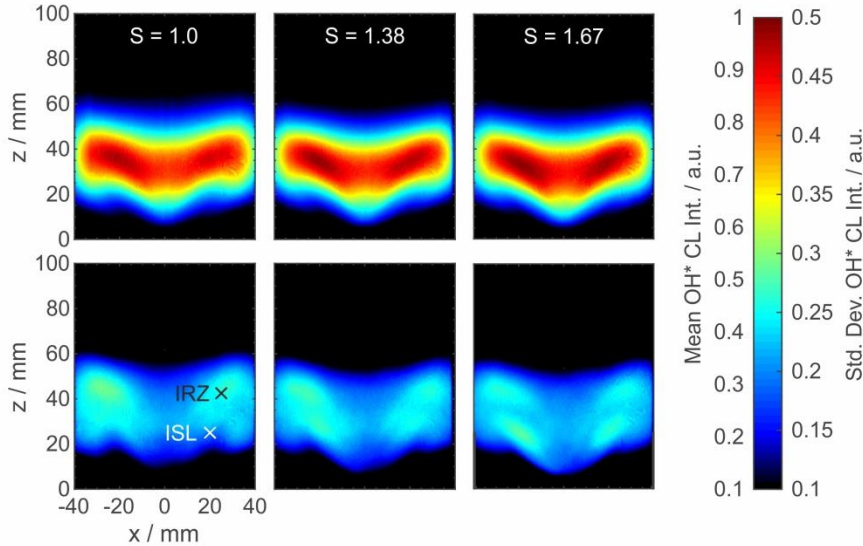


Figure 3. Mean (top row) and standard deviation (bottom row) of the  $\text{OH}^*$  chemiluminescence signal for the different stratification ratios. The black and white crosses mark the positions where the FFTs of the fluctuations in the inner recirculation zone (IRZ) and inner shear layer (ISL), respectively, were evaluated (discussed below).

Here, the mean and standard deviation of the  $\text{OH}^*$  chemiluminescence (CL) signal are shown. The flame shape is similar for all operating conditions. All flames feature a V-shape and the apex is approximately  $90^\circ$  for all flames. The flame root is lifted approximately 10 mm from the nozzle, while the main flame zone is between 30 mm and 40 mm above the nozzle. The standard deviation for the  $\text{OH}^*$  CL however differs for the three studied operating conditions. While for  $S = 1.0$ , the standard deviation seems more homogeneously distributed, for  $S = 1.38$  and  $S = 1.67$ , an area with low  $\text{OH}^*$  CL fluctuations is observed between the inner shear layer (ISL) and inner recirculation zone (IRZ), which becomes more pronounced with increasing  $S$ . Apart from this feature, however, all studied flames behave similarly. The origin of those fluctuations will be discussed below.

## Flow Field

Figure 4 shows the mean (top row) and standard deviation (bottom row) of the axial velocity component. Overlaid are the streamlines. Like the mean flame zone, derived from the  $\text{OH}^*$  CL images, the mean velocity field is similar for all studied flames. The flow field is typical for swirl stabilized flames, featuring a high velocity inflow region, enclosed by an inner (ISL) and outer (OSL) shear layer, and inner (IRZ) and outer (ORZ) recirculation zones. The main velocity fluctuations are observed in the shear layers.

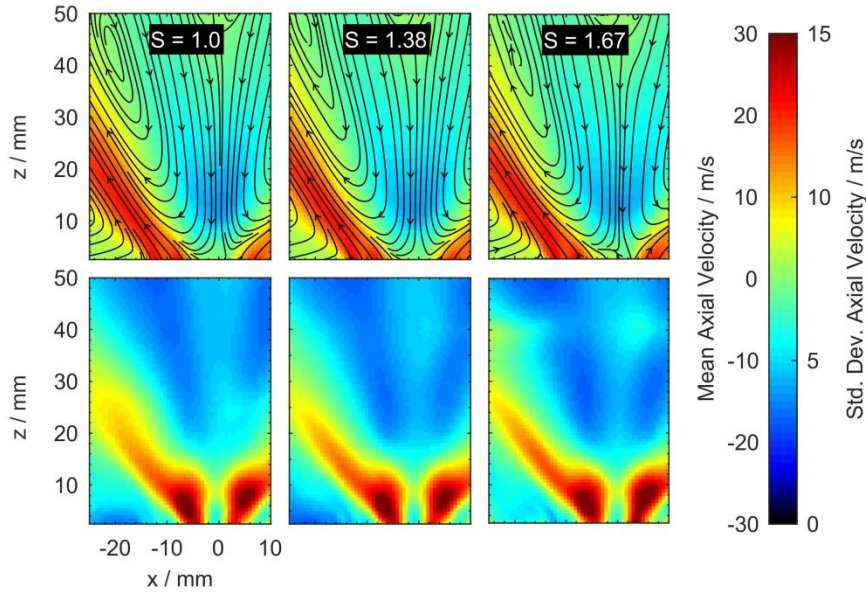


Figure 4. Mean (top row) and standard deviation (bottom row) of the axial velocity component. Overlaid are the streamlines.

An area of increased velocity fluctuations appears on the symmetry axis ( $x = 0$  mm) at an axial location of approximately  $z = 40$  mm and increases in strength with increasing  $S$ . This could be a part of the exhaust tube vortex [26], which forms due to the contraction at the end of the combustion chamber.

Figure 5 shows scatterplots of mixture fraction vs. temperature gained using laser Raman scattering at  $z = 8$  mm and  $z = 15$  mm for  $S = 1.67$ . Color coded is the radial location of the measurements.

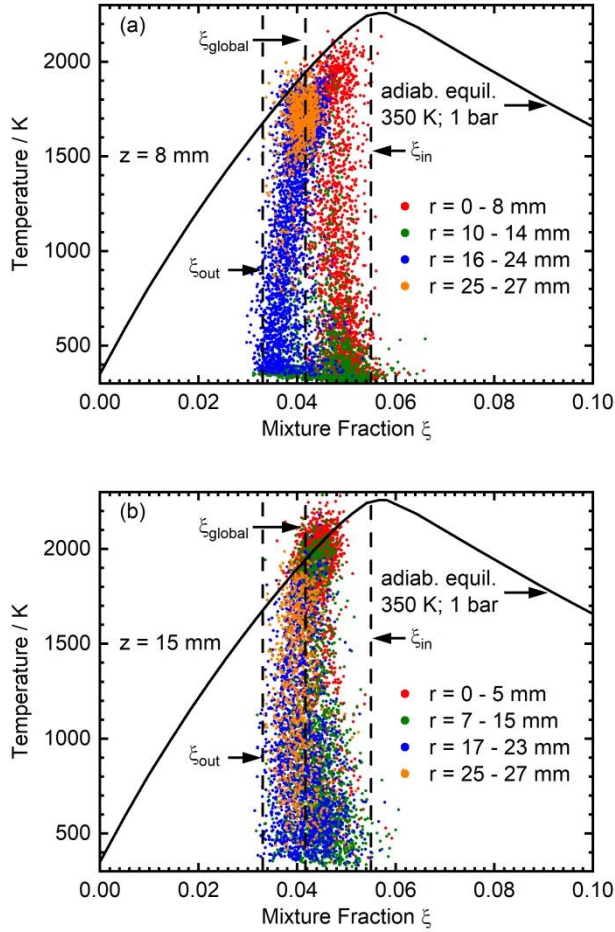


Figure 5. Scatterplot of mixture fraction vs. temperature for (a)  $z = 8$  mm and (b)  $z = 15$  mm for  $S = 1.67$ . Color coded is the radial position of the individual samples. The vertical dashed lines correspond to the global mixture fraction, and the mixture fractions of the inner and outer swirler, the solid black line corresponds to the adiabatic equilibrium for a fresh gas temperature of 350 K.

At  $z = 8$  mm, samples originating from the inner and outer swirler can clearly be distinguished, especially for the radial bins  $0 \text{ mm} < x < 8 \text{ mm}$  and  $10 \text{ mm} < x < 14 \text{ mm}$ , as the two streams have not mixed completely at this axial location. However, samples with mixture fractions corresponding to the inlet condition of the inner or outer swirler are only observed for unreacted samples: Most reacted samples show a certain degree of mixing or are fully mixed. For  $10 \text{ mm} < x < 14 \text{ mm}$ , most samples are unreacted, while for  $25 \text{ mm} < x < 27 \text{ mm}$ , most samples are completely reacted and near the global

mixture fraction. For  $0 \text{ mm} < x < 8 \text{ mm}$  and  $16 \text{ mm} < x < 24 \text{ mm}$ , a large number of samples in an intermediate state are observed.

At  $z = 15 \text{ mm}$ , all observed samples are close to the global mixture fraction. Here as well reacted, unreacted and intermediate samples are observed for most radial locations. Only for  $0 \text{ mm} < x < 5 \text{ mm}$ , most samples are completely reacted.

All examined flames feature strong self-excited thermo-acoustic oscillations. The overall sound pressure level in the combustion chamber increases with increasing stratification ratio from  $p' \approx 370$  Pa at  $S = 1$  to  $p' \approx 460$  Pa at  $S = 1.67$ . Several distinct modes with different amplitudes occur in the frequency spectrum of both the pressure in the combustion chamber and two plenums as well as in the integrated OH\* CL signal.

Table 2 shows an overview of all observed thermo-acoustic modes at different locations within the combustor and for different measurement quantities, as well as the physical origin of the individual modes. Furthermore, the trend of the individual modes with increasing  $S$  is depicted.

*Table 2. Frequencies of the observed thermo-acoustic modes and their physical meanings, as well as their occurrence in different locations of the combustor and measured quantities as well as their trend with varying  $S$ . HOP corresponds to the Helmholtz-mode of the outer plenum with the combustion chamber, OP1, OP2, IP1, and IP2 are Eigenmodes of the inner and outer plenum, respectively. PVC is the mode corresponding to the precessing vortex core.  $u$  is the axial velocity component at  $z = 5$  mm at the centerline (C) and in the inner (inSw) and outer (outSw) swirler. An upper case “X” denotes a strong occurrence of the mode, a lower case “x” a weak occurrence of the mode and a “-” no occurrence of the mode.*

f / Hz	Mode	IP	OP	CC	CL	$u_C$	$u_{inSw}$	$u_{outSw}$	$\uparrow S$
180	HOP	X	X	X	X	-	-	x	$\uparrow$
400	OP1	X	X	X	X	-	-	x	$\uparrow$
455	IP1	x	x	x	X	-	x-	-	$\downarrow$
700	OP2	X	X	X	X	-	-	x	$\uparrow$
756	IP2	-	-	-	x	-	x	-	$\uparrow$
880	HOP + OP2	x	x	x	-	-	-	-	-
1160	PVC	x	X	x	X	X	X	X	-
1340	PVC + HOP	x	x	X	x	x	x	x	$\uparrow$
1600	PVC + IP1	X	-	-	x	-	x	-	$\uparrow$
1860	PVC + OP2	X	-	x	x	-	-	x	$\uparrow$

The identification of the individual modes is based on, numerical modelling of the Eigenmodes of the combustion chamber and plenums, which was performed in a previous study [15] in order to identify the origin of different acoustic Eigenmodes of the system. HOP corresponds to the Helmholtz-mode of



the outer plenum with the combustion chamber, OP1, OP2, IP1, and IP2 are Eigenmodes of the inner and outer plenum, respectively. PVC is the mode corresponding to the precessing vortex core. The frequency spectra of the pressure oscillations in the combustion chamber as well as in the inner and outer plenum for the perfectly premixed flame with a stratification ratio  $S = 1$  are shown in Figure 6.

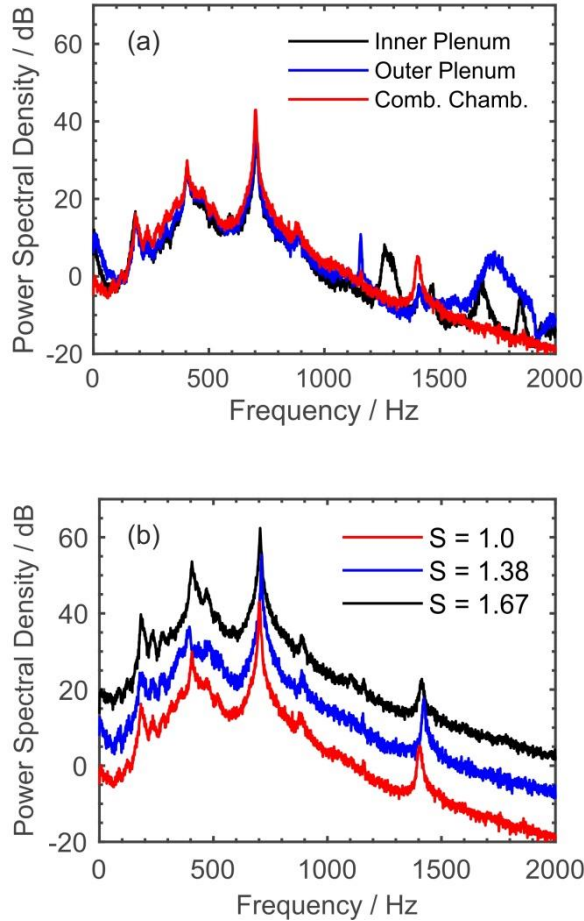


Figure 6. (a) Acoustic spectra of the inner and outer plenum as well as the combustion chamber for  $S = 1$ . (b) Acoustic spectra of the combustion chamber for the different stratification ratios. For a better overview, the spectra are shifted by 10 dB.

The dominant frequency both in the combustion chamber and in the two plenums is observed at  $f_{TA} = 700$  Hz. This mode corresponds to an Eigenmode of the outer plenum and is similar in amplitude for all flames. At approximately  $f_{OP1} \approx 400$  Hz, the mode corresponding to an Eigenmode of outer plenum occurs in both plenums and in the combustion chamber. Furthermore, a precessing vortex core (PVC) at with  $f_{PVC} \approx 1165$  Hz is seen most dominantly in the frequency spectrum of the outer plenum, but also visible in the frequency spectrum of the combustion chamber. Further dominant modes include the Helmholtz mode of the combustion chamber and the outer plenum at approximately  $f_{HOP} = 180$  Hz

and a mode at approximately  $f = f_{\text{HOP}} + f_{\text{TA}} = 880$  Hz, which is the sum frequency of the main thermo-acoustic mode and the Helmholtz mode of the outer plenum.

The frequency spectra of the acoustic oscillations in the combustion chamber for the different stratification ratios are shown in Figure 6b. Here, the spectra are similar in shape. However, the amplitudes at some characteristic frequencies differ for the different stratification ratios, mainly at 180 Hz.

A good overview of the (global and local) dynamic behavior of the different flames is gained by performing a pixel-wise fast Fourier transform (FFT) of the  $\text{OH}^*$  CL signal, which is shown in Figure 7.

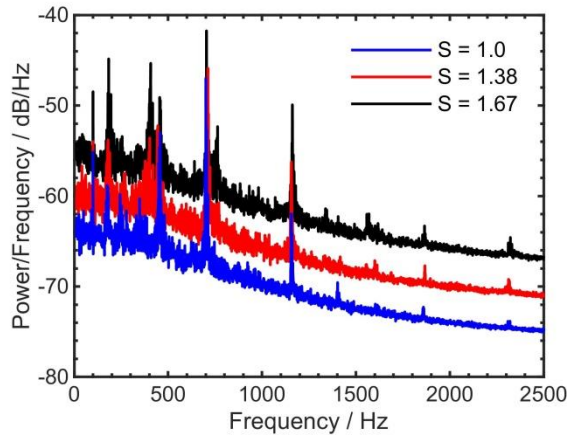


Figure 7. Frequency spectrum of global and local variations of the  $\text{OH}^*$  chemiluminescence signal.

Here, a separate FFT was performed for each pixel of the  $\text{OH}^*$  CL image frames. The resulting FFTs were averaged to increase the signal-to-noise ratio. Thus, dominant frequencies of both global modes (such as thermo-acoustics) and local / asymmetric modes (e.g. precessing vortex cores, which influence the heat release distribution, but not necessarily the total heat release) can be identified. Here, the most dominant mode is at the main thermo-acoustic oscillation of  $f_{\text{TA}} = 700$  Hz and is similar in amplitude for all flames. The sharp peak at 100 Hz is an artifact of the data processing.

The PVC at  $f_{\text{PVC}} \approx 1165$  Hz can also be observed in the  $\text{OH}^*$  CL, indicating a strong interaction of this coherent flow structure with the flame. The sum-frequency of the dominant mode at  $f_{\text{TA}} = 700$  Hz and the PVC ( $f_{\text{PVC}} = 1165$  Hz) is observed at 1865 Hz. The peak corresponding to this frequency increases in strength with decreasing  $S$ , indicating that the interaction between the PVC and the thermo-acoustic oscillation is strongest for the perfectly premixed case. Additional modes visible in the amplitude

spectrum of the  $\text{OH}^*$  CL are at approximately  $f_{\text{HOP}} = 180$  Hz (corresponding to the Helmholtz mode of the combustion chamber and the outer plenum). This mode is strongly influenced by the stratification ratio: it is weakest for the perfectly premixed case and increases in strength with increasing stratification. An additional strong mode at  $f_{\text{OP1}} \approx 400$  Hz, whose amplitude and frequency increase with increasing  $S$ , corresponds to the first Eigenmode of outer plenum. In a similar frequency range, the first Eigenmode of the inner plenum at  $f_{\text{IP1}} \approx 450$  Hz is visible, with an increasing amplitude with decreasing  $S$ . The mode at  $f_{\text{OP2}} \approx 760$  Hz corresponds to a second Eigenmode of the inner plenum and increases in amplitude with increasing  $S$ .

In order to gain insight into the local dynamics of the  $\text{OH}^*$  CL and the regions of high standard deviation in the inner shear layer (ISL) and at the edge of the inner recirculation zone (IRZ), FFTs were performed in those regions (IRZ,  $x = 25$  mm,  $z = 42.5$  mm) and in the outer shear layer (ISL,  $x = 20$  mm,  $z = 25$  mm). The resulting FFTs are shown in Figure 8.

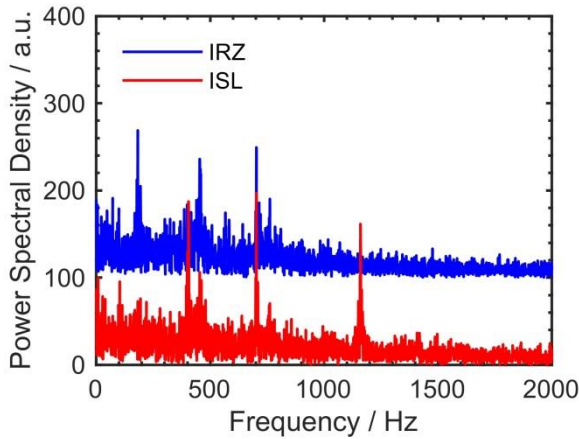


Figure 8. FFTs of the  $\text{OH}^*$  CL signal in the inner shear layer (ISL) and inner recirculation zone (IRZ) for  $S = 1.67$ .

The dominant mode in the inner recirculation zone is at 180 Hz, and additional modes with similar amplitudes are present at 700 Hz and 455 Hz. A further mode at 760 Hz features a lower amplitude.

In the inner shear layer, the mode at 700 Hz dominates the frequency spectrum. However, a mode at 400 Hz and a mode at 1165 Hz are similar in amplitude. Modes at 455 Hz and 760 Hz also occur, but with lower amplitudes.

In summary, the stratification level has a clear influence on the thermo-acoustic and heat release fluctuations of the current configuration. While all flames feature the same most dominant mode, with

similar pressure and heat release fluctuation amplitudes, several less dominant modes are only present for certain stratification levels or vary in amplitude, depending on the stratification level.

### *Velocity Coupling*

In order to determine the influence of the observed acoustic and HRR oscillation modes on the flow field, frequency spectra of the radial velocity component were performed at  $z = 5$  mm since the characteristic frequencies are best visible in the radial velocity component. The corresponding spectra at different radial locations, namely the centerline of the combustion chamber ( $x = 0$  mm), at the center of the radius of the inner nozzle ( $x = 3.75$  mm) and at the center of the radius of the outer nozzle ( $x = 9.75$  mm), are shown in Figure 9.

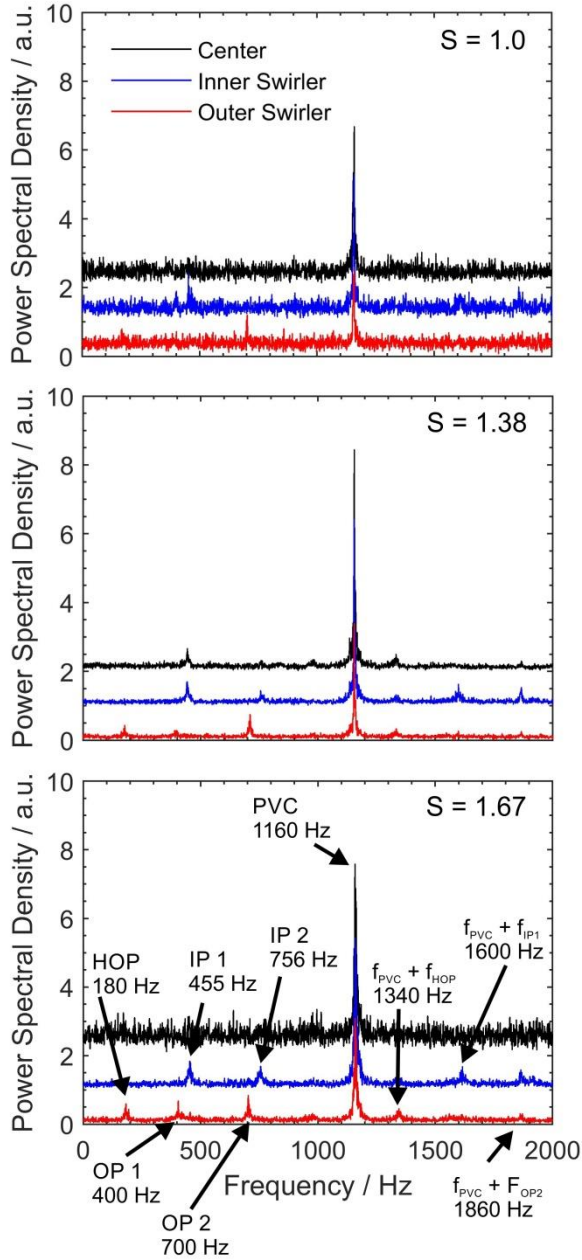


Figure 9. Frequency spectra of the radial velocity component at  $z = 5$  mm and radial locations corresponding to the centerline of the combustion chamber (black curve), the center of the radius of the inner air nozzle (blue curve) and the center of the radius of the outer air nozzle (red curve). HOP corresponds to the Helmholtz mode of the combustion chamber with the outer plenum, PVC corresponds to the frequency of the precessing vortex core. IP 1, IP2, OP1 and OP2 correspond to Eigenmodes of the inner and outer plenum, respectively.

The dominant frequency of  $f_{PVC} \approx 1165$  Hz of the radial velocity component corresponds to the precessing vortex core (PVC). This mode is dominant for all stratification ratios. For the perfectly premixed case ( $S = 1$ ), the PVC is the only dominant mode at the combustor centerline. In the inflow of the inner swirler, further modes at  $f_{IP1} = 455$  Hz (corresponding to an Eigenmode of the inner plenum) and at  $f = f_{PVC} + f_{OP2} = 1860$  Hz (corresponding to the sum frequency of the PVC and an Eigenmode of

the outer plenum) are visible. In the inflow of the outer swirler, a mode at  $f_{OP2} = 700$  Hz (corresponding to an Eigenmode of the outer plenum) and a very weak mode at  $f_{HOP} = 180$  Hz (corresponding to the Helmholtz mode of the outer plenum with the combustion chamber) can be observed.

With increasing stratification ratio, several additional modes appear, while some existing modes increase in strength. One mode with a strong sensitivity on the stratification ratio is the Helmholtz mode of the outer plenum and the combustion chamber, which increases in amplitude with increasing  $S$ , mainly visible in the frequency spectrum of the flow of the outer swirler. Two Eigenmodes of the outer plenum (OP1 and OP2) also become visible with increasing stratification ratio. Also one mode of the inner plenum (IP2) appears with increasing  $S$ . Since the mixture in the outer stream becomes leaner with decreasing  $S$ , the observed increased thermo-acoustic instability of the flame (represented by the occurrence of additional modes) could be due to an increased instability of the flame due to a lower local equivalence ratio. Thus, the flame in this region is more prone to instabilities.

#### *Thermo-Acoustic Feedback Regions*

Next, the distinct modes of the flame shape, represented by the OH LIF distributions, are considered. To give an overall impression of the shape of the OH distribution, Figure 10 displays a mean OH PLIF distribution in the same plane as the velocity distributions of Figure 4, averaged over 30,000 single shots for the flame with  $S = 1.67$ .

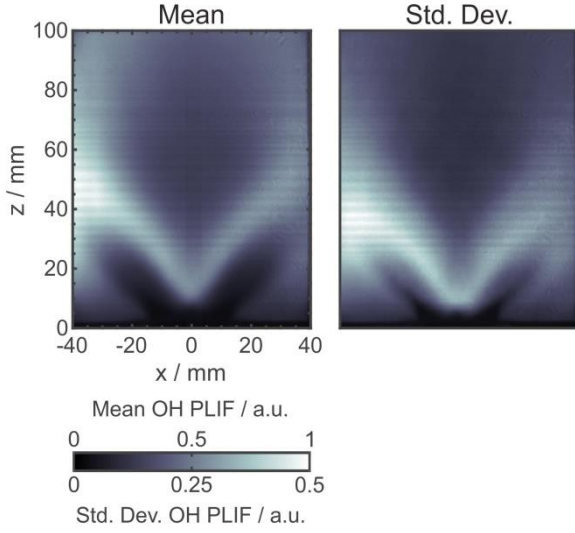


Figure 10. Normalized mean (left) and standard deviation (right) of the OH PLIF signal for  $S = 1.67$ .

The OH-free regions close to the nozzle reflect the inflow of fresh gas. The regions with high signal levels represent the flame brush where high temperatures and super-equilibrium OH concentrations are present. These regions coincide well with the  $\text{OH}^*$  chemiluminescence distributions of Figure 3 if those are Abel-transformed to yield a quasi-2D cut through the flame (not displayed). Further downstream, at heights above  $z \approx 50$  mm, the OH LIF signals represent hot exhaust gas that slowly cools down by contact with the combustion chamber wall. A similar cooling effect is seen for the reacted gas containing OH in the ORZ.

For the series of single shot OH PLIF distributions of the three flames, a FFT was performed for each pixel, and the most dominant frequency (determined by the maximum amplitude) and the second most dominant mode (determined by the second highest amplitude) were extracted pixel-wise. The results are displayed in Fig. 11 as 2D-distributions. The regions of the inflow, where hardly any OH was detected, are masked in these illustrations.

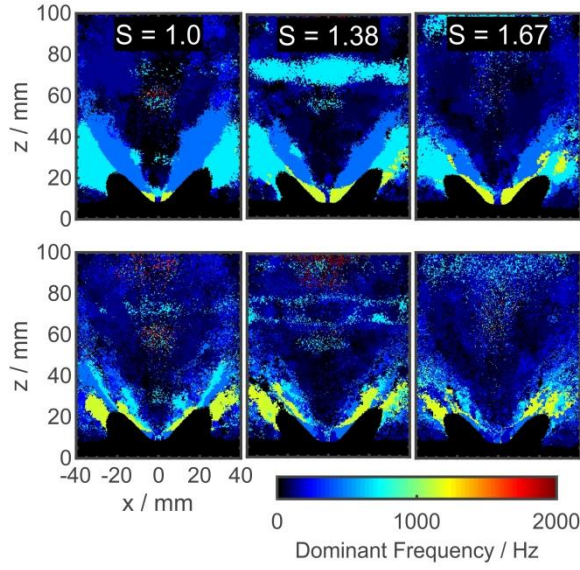


Figure 11. Dominant (top row) and second dominant (bottom row) frequency of the OH PLIF signal. The light blue regions correspond to a frequency of 700 Hz, the dark blue regions to a frequency of 455 Hz. The even darker blue regions correspond to a frequency of 400 Hz. The yellow regions correspond to the PVC frequency of 1165 Hz.

The light blue regions correspond to domains where the main thermo-acoustic mode at 700 Hz (OP2) is dominant, the medium blue regions correspond to areas, where the first Eigenmode of the inner plenum ( $f_{IP1} \approx 455$  Hz) is dominant, regions in dark shade of blue reflect the dominance of the mode OP1 ( $\approx 400$  Hz) (see Figure 6, Figure 7 and Figure 9). The yellow regions reflect areas, where the PVC ( $f_{PVC} \approx 1165$  Hz) dominates the OH variations. For all flames, the most dominant mode in the ISL, where the flame resides, is at 455 Hz. This shows that the position of the flame responds to the oscillation coupled to the inner plenum. However, the dominance of this mode decreases in spatial extent with increasing  $S$ . One reason for the change is certainly that with increasing  $S$  the mode OP1 at 400 Hz comes into play (see Figure 6 and Figure 7). The dominant mode in the OSL and ORZ is at 700 Hz, i.e. the strongest thermo-acoustic mode. It is plausible that this mode exhibits the strongest thermo-acoustic level, because it is coupled to the outer plenum from where most of the fuel is supplied. Also, the decrease of OH\* signal of this mode with increasing  $S$  (see Figure 7) corresponds to the decrease of fuel in the outer plenum. It is further seen that the PVC has a significant influence on the OH PLIF fluctuations, particularly close to the anchor region of the flames at  $z \approx 10 - 20$  mm close to the flame axis. Here, the PVC rotates the flame around the axis. The bottom row of Figure 11 with the second dominant frequencies of the OH PLIF signals does not convey a clear picture. However, together with



the upper row it illustrates that the most dominant modes are everywhere present in the OH-containing regions.

## Summary

A dual swirl gas turbine model combustor was operated with different premixed compositions of  $\text{CH}_4$  and air in the two swirling flows to study the influence of stratification on the flame behavior. Laser, optical and acoustic measurements were performed to gain information about temperature, species concentration, and flow field and flame dynamics under those combustion conditions. The analysis of the thermo-chemical state of the flame showed that mixture stratification was mainly present at and below the flame root, while the mixture is more homogenous downstream of the flame root and within the main flame zone. All examined flames featured significant self-excited thermo-acoustic oscillations at different frequencies with a dominant frequency at 700 Hz. The different modes could be identified in the pressure traces within the plenums and the combustion chamber as well as in the chemiluminescence intensities and velocity fluctuations. Most of these modes were attributed to resonances with the inner or outer plenum. Changing the stratification level had only a minimal influence on the mean values of flame shape and flow field. However, a clear influence on the thermo-acoustic oscillations, on the flow dynamics, and on the flow-flame interaction (i.e. the interaction between the flame and a precessing vortex core (PVC)) was identified. The amplitudes of the different modes changed with the stratification ratio; most modes increased in strength with increasing stratification ratio, while some were attenuated. A mode analysis of the distributions of the OH radical revealed that different modes were dominant in different regions of the flame. The PVC frequency was clearly visible, not only in the velocity fluctuation spectra, but also in the  $\text{OH}^*$  chemiluminescence and pressure spectra. Its influence decreased with increasing stratification ratio. The spatial distributions of the dominant modes correlated with the location of the corresponding flows and their resonances from the inner or outer swirler.

It was clearly seen that the stratification influenced the level and the spectral composition of the sound emissions. The dominant mode in the outer shear layer and outer recirculation zone is at 700 Hz, i.e. the strongest thermo-acoustic mode. It is assumed that this mode exhibits the highest fluctuation amplitude, because it is coupled to the outer plenum from where most of the fuel is supplied. Also, the decrease of  $\text{OH}^*$  signal of this mode with increasing  $S$  corresponds to the decrease of fuel in the outer plenum. In

future work, it will be investigated how the spectral distribution and the attenuation of acoustic emissions can be specifically controlled by stratification.

## Acknowledgement

The financial support by the German Research Council (DFG) within the Collaborative Research Center 606 is gratefully acknowledged. Michael Severin and Yawei Gao are acknowledged for their help in setting up the experiment.

## Conflict of Interest

The authors declare that they have no conflict of interest.

## References

1. Biagioli, F.: Stabilization mechanism of turbulent premixed flames in strongly swirled flows. *Combustion Theory and Modelling* **10**(3), 389-412 (2006). doi:<https://doi.org/10.1080/13647830500448347>
2. Lazik, W., Doerr, T., Bake, S., v. d. Bank, R., Rackwitz, L.: Development of Lean-Burn Low-NOx Combustion Technology at Rolls-Royce Deutschland. (43130), 797-807 (2008). doi:<https://10.1115/GT2008-51115>
3. Sweeney, M.S., Hochgreb, S., Barlow, R.S.: The structure of premixed and stratified low turbulence flames. *Combust. Flame* **158**, 935-948 (2011). doi:<https://doi.org/10.1016/j.combustflame.2011.02.007>
4. Sweeney, M.S., Hochgreb, S., Dunn, M.J., Barlow, R.S.: The structure of turbulent stratified and premixed methane/air flames II: Swirling flows. *Combust. Flame* **159**, 2912-2929 (2012). doi:<https://doi.org/10.1016/j.combustflame.2012.05.014>
5. Sweeney, M.S., Hochgreb, S., Dunn, M.J., Barlow, R.S.: The structure of turbulent stratified and premixed methane/air flames I: Non-swirling flows. *Combust. Flame* **159**, 2896-2911 (2012). doi:<https://doi.org/10.1016/j.combustflame.2012.06.001>
6. Seffrin, F., Fuest, F., Geyer, D., Dreizler, A.: Flow field studies of a new series of turbulent premixed stratified flames. *Combust. Flame* **157**(2), 384-396 (2010). doi:<https://doi.org/10.1016/j.combustflame.2009.09.001>
7. Kuenne, G., Seffrin, F., Fuest, F., Stahler, T., Ketelheun, A., Geyer, D., Janicka, J., Dreizler, A.: Experimental and numerical analysis of a lean premixed stratified burner using 1D Raman/Rayleigh scattering and large eddy simulation. *Combust. Flame* **159**(8), 2669-2689 (2012). doi:<https://doi.org/10.1016/j.combustflame.2012.02.010>
8. Meares, S., Masri, A.R.: A modified piloted burner for stabilizing turbulent flames of inhomogeneous mixtures. *Combust. Flame* **161**(2), 484-495 (2014). doi:<https://doi.org/10.1016/j.combustflame.2013.09.016>
9. Meares, S., Prasad, V.N., Magnotti, G., Barlow, R.S., Masri, A.R.: Stabilization of piloted turbulent flames with inhomogeneous inlets. *Proc. Combust. Inst.* **35**(2), 1477-1484 (2015). doi:<https://doi.org/10.1016/j.proci.2014.05.071>
10. International Workshop on the Measurement and Computation of Turbulent Flames (TNF). <https://tnfworkshop.org/>.
11. Masri, A.R.: Partial premixing and stratification in turbulent flames. *Proc. Combust. Inst.* **35**(2), 1115-1136 (2015). doi:<https://doi.org/10.1016/j.proci.2014.08.032>

12. Huang, Y., Yang, V.: Dynamics and stability of lean-premixed swirl-stabilized combustion. *Prog. Energy Combust. Sci.* **35**(4), 293-364 (2009). doi:<https://doi.org/10.1016/j.pecs.2009.01.002>
13. Weigand, P., Meier, W., Duan, X.R., Stricker, W., Aigner, M.: Investigations of swirl flames in a gas turbine model combustor I. Flow field, structures, temperature, and species distributions. *Combust. Flame* **144**(1-2), 205-224 (2006). doi:<https://doi.org/10.1016/j.combustflame.2005.07.010>
14. Meier, W., Weigand, P., Duan, X.R., Giezendanner-Thoben, R.: Detailed characterization of the dynamics of thermoacoustic pulsations in a lean premixed swirl flame. *Combust. Flame* **150**(1-2), 2-26 (2007). doi:<https://doi.org/10.1016/j.combustflame.2007.04.002>
15. Arndt, C.M., Severin, M., Dem, C., Stöhr, M., Steinberg, A.M., Meier, W.: Experimental analysis of thermo-acoustic instabilities in a generic gas turbine combustor by phase-correlated PIV, chemiluminescence, and laser Raman scattering measurements. *Exp. Fluids* **56**(4), 69 (2015). doi:<https://doi.org/10.1007/s00348-015-1929-3>
16. Meier, W., Dem, C., Arndt, C.M.: Mixing and reaction progress in a confined swirl flame undergoing thermo-acoustic oscillations studied with laser Raman scattering. *Exp. Therm. Fluid Sci.* **73**, 71-78 (2015). doi:<https://doi.org/10.1016/j.expthermflusci.2015.09.011>
17. Arndt, C.M., Stöhr, M., Severin, M.J., Dem, C., Meier, W.: Influence of air staging on the dynamics of a precessing vortex core in a dual swirl gas turbine model combustor. In: 53rd AIAA/SAE/ASME Joint Propulsion Conference 2017. AIAA Propulsion and Energy Forum, AIAA 2017-4683. doi:<https://doi.org/10.2514/6.2017-4683>
18. Arndt, C.M., Steinberg, A.M., Böhnke, J., Hadeff, R., Meier, W.: High Speed Imaging of Flame Structure and Dynamic Processes in Swirl Stabilized Pre-vaporized Liquid Fuel Flames. In: AIAA Scitech Forum 2019, AIAA 2019-0732. doi:<https://doi.org/10.2514/6.2019-0732>
19. Arndt, C.M., Steinberg, A.M., Meier, W.: Flame Extinction and Re-Ignition in a Swirl Stabilized Pre-vaporized Liquid Fuel Flame Close to Lean Blow-Out. In: AIAA Scitech Forum 2020, AIAA 2020-1879. doi:<https://dx.doi.org/10.2514/6.2020-1879>
20. Bärow, E., Koch, R., Bauer, H.-J.: Comparison of oscillation modes of spray and gaseous flames. In: Proceedings of the Eighth Mediterranean Combustion Symposium 2013, EGTSC-26.
21. Kraus, C., Harth, S., Bockhorn, H.: Experimental investigation of combustion instabilities in lean swirl-stabilized partially-premixed flames in single- and multiple-burner setup. *International Journal of Spray and Combustion Dynamics* **8**(1), 4-26 (2016). doi:<https://doi.org/10.1177/1756827715627064>
22. Keck, O., Meier, W., Stricker, W., Aigner, M.: Establishment of a Confined Swirling Natural Gas/Air Flame as a Standard Flame: Temperature and Species Distributions from Laser Raman Measurements. *Combustion Science and Technology* **174**(8), 117-151 (2002). doi:<https://doi.org/10.1080/713713067>
23. Bergmann, V., Meier, W., Wolff, D., Stricker, W.: Application of spontaneous Raman and Rayleigh scattering and 2D LIF for the characterization of a turbulent CH<sub>4</sub>/H<sub>2</sub>/N<sub>2</sub> jet diffusion flame. *Appl. Phys. B* **66**(4), 489-502 (1998). doi:<https://doi.org/10.1007/s003400050424>
24. Bilger, R.W., Starnes, S.H.: On reduced mechanisms for methane/air combustion in nonpremixed flames. *Combust. Flame* **80**(2), 135-149 (1990). doi:[https://doi.org/10.1016/0010-2180\(90\)90122-8](https://doi.org/10.1016/0010-2180(90)90122-8)
25. Duan, X.R., Meier, W., Weigand, P., Lehmann, B.: Phase-Resolved Laser Raman Scattering and Laser Doppler Velocimetry Applied to Periodic Instabilities in a Gas Turbine Model Combustor. *Appl. Phys. B* **80**, 389-396 (2005). doi:<https://doi.org/10.1007/s00340-004-1722-0>
26. Stöhr, M., Boxx, I., Carter, C.D., Meier, W.: Experimental study of vortex-flame interaction in a gas turbine model combustor. *Combust. Flame* **159**(8), 2636-2649 (2012). doi:<https://doi.org/10.1016/j.combustflame.2012.03.020>